Hindawi
Mathematical Problems in Engineering
Volume 2020, Article ID 5783653, 13 pages
https://doi.org/10.1155/2020/5783653

Research Article

Structural and Mechanical Characteristics of a Capsule-Type Soft Pneumatic Actuator with Large Thrust Force and High-Contraction Ratio

Qing Zhu,[1] Qingyun Liu,[1] Mingxing Yang,[2] and Xingsong Wang[2]

[1]*School of Mechanical Engineering, Anhui University of Technology, Ma'anshan 243002, China*
[2]*School of Mechanical Engineering, Southeast University, Nanjing 211189, China*

Correspondence should be addressed to Xingsong Wang; xswang@seu.edu.cn

Received 30 December 2019; Accepted 19 March 2020; Published 30 April 2020

Academic Editor: Michele Guida

A capsule-type soft pneumatic actuator (CTSPA) was molded with hyperelastic material (latex) and subjected to deformations. In order to provide a large thrust force and limit the direction of expansion and contraction, the actuator was covered by fiber materials and driven by compressed air. Soft pneumatic actuator, belonging to flexible drive, showed nonlinear characteristics. In this study, with theoretical and experimental methods, a static mathematical model of CTSPA was established to analyze the relationship between the inflation pressure, driving force, and deformations. Furthermore, we experimentally explored the response characteristics of CTSPA by using a unit step function. The hysteresis was significantly affected by air pressure, loading size, and effective contact area of the actuator. Finally, the actuator realized a compatible position tracking performance of 1 Hz and a low average tracking error of 0.3°. The study provides a basis for studying the control methods and state maintenance of flexible drive systems.

1. Introduction

Soft robots, made with soft or flexible materials, mimic the material, mechanics, morphological structure, and motion characteristics of soft organisms in nature. Soft robots have the characteristics of safety, suppleness, high flexibility, and complex environmental adaptability. Soft robotics technology has been widely concerned at home and abroad [1, 2] since it has great application potential in minimally invasive surgery, massage therapy rehabilitation, disaster relief, and military fields.

The domestic and foreign scholars' inspiration for soft robots comes from all kinds of invertebrate mollusks and arthropods in nature, including their shapes and movement postures. Soft robots are generally made with soft and hyperelastic materials, such as rubber, shape memory alloy (SMA), electroactive polymer (EAP), and reaction hydrogel. By changing its own structural shape and size, soft robots can be adapted to the nonstructural working environment and have the extensive application and development prospects in rehabilitation, military battlefield, and disaster relief.

Pneumatic Muscle Actuator (PMA), invented by Mchibben, is a mature soft-driven technology. It has similar mechanical properties to biological muscles, such as high power/mass ratio and high power/volume ratio, and has been applied in a variety of robots providing driving force. Since it can contract only in one direction, it needs to be used in pairs to generate two-way forces or motions, and its contraction ratio is generally 20%~40% [3]. With hyperelastic material silicone, Tolley et al. [4] developed a simulated starfish soft robot, which used an air compressor to provide the power for both creep and undulation movements. Galloway et al. [5] built a fluid channel in the robot body made with hyperelastic materials and embedded in the fiber-reinforced layer to control the bending of the soft robot by controlling the volume of the fluid in the channel. Wang et al. [6] developed a pneumatic honeycomb network soft actuator with large deformation, high flexibility, and a high

load-to-weight ratio, which paved a new way for eliminating the inherent limitations of rigid robots. Bartlett et al. [7] used the three-dimensional printing technology to create an internal combustion-driven robot, which used the energy released in chemical reactions as a driving mechanism to drive the robot to jump, and achieved a directional jump by inflating the feet at the bottom. Wehner et al. [8] prepared the first all-soft robot in the world with 3D printing technology to provide the power required by chemical reactions.

Pneumatic artificial muscle is a kind of flexible gas-driven driving device and has been widely applied in many fields, especially medical, magnetic, limited space, and other applications, to provide a strong contraction pull force. The static mathematical model of pneumatic artificial muscle is the basis for the study and application of PMA drives. Chou and Hannaford [9] established an ideal mathematical model of PMA based on the principle of conservation of energy and other scholars further improved the model [10–14]. Li et al. [15, 16] improved and verified the mathematical model of pneumatic artificial muscles. Teng et al. [17] proposed a pneumatically elongated pneumatic flexible actuator and explored its characteristics, but its structure size was too large and not suitable for confined spaces. Belforte et al. [18] provided an innovative bellows textile muscle and evaluated its performances with both analytic and numerical models. Lee and Rodrigue [19] proposed an origami-based vacuum pneumatic artificial muscle with a large contraction ratio to produce large forces and developed a quasistatic analytical model to accurately predict the behavior of the actuator. Yang et al. [20] developed a high-displacement pneumatic artificial muscle made with textiles or plastics with larger contraction ratios and presented a model for the specified forces and displacement design.

Soft robots are generally made with soft and elastic materials with nonlinear characteristics, so it is of great significance to study their dynamic response characteristics [21–26]. Soft pneumatic actuators convert the energy of gas into mechanical energy. It is an executive element of the pneumatic transmission system and can provide displacement and thrust force during the operation. The dynamic characteristics of the soft pneumatic actuator, the inflating and exhausting characteristics, are an important indicator of the performance of the pneumatic drive system. The dynamic response characteristics of the actuator are the basis for the control and application of the soft pneumatic actuator. Sarosi et al. [27] developed a new dynamic model for an actuator as a pneumatic artificial muscle (PAM) with two-directional motion and found that the dynamic properties of the system were close to the experimentally determined characteristics. Veale et al. [28] proposed a novel planar fluidic artificial muscle and analyzed its static and dynamic behaviors by a parallel ideal contractile unit and viscoelastic element.

Considering that conventional pneumatic actuators cannot simultaneously realize both a high-contraction ratio and a large thrust force, we proposed a capsule-type soft pneumatic actuator (CTSPA). The actuator was molded by superelastic material (latex) and covered with fiber material, so it had a high contraction ratio and can provide a large thrust force. The soft actuator structure was safe and soft and had the controllable contact force. Capsule-type balloon (made of latex) is a good choice due to its large expansion ratio and output thrust. Therefore, in this paper, the latex balloon covered with the fiber material as the structure of the soft pneumatic actuator and the mechanical characteristics were explored.

2. Structural Characteristics and Working Principle of CTSPA

Latex balloons as inflatable expansion drive devices are widely applied in medical rehabilitation equipment such as sphygmomanometers and massage chairs. In addition, car airbags, vibration-damping air springs, aircraft landing cushions, etc. are also characterized by the inflation of the bladder. The actuator selected in this study is made with latex with good ductility and not easy to blast. When the actuator is inflated, the air pressure in the balloon chamber is increased, so that the balloon is expanded to provide driving force and displacement. In order to improve the driving force from the balloon, the outer surface of the balloon is covered with a layer of fiber material to limit the expansion volume, as shown in Figure 1.

The structural parameters of the actuator are provided as follows:

Length—a

Width—b

Wall thickness—d

Length of the covering fiber cloth—a_1

Width of the covering fiber cloth—b_1

Initial volume of the actuator $V_1 = 2abd$

During the working period, a load is firstly applied above the actuator and then a displacement occurs under the inflation and contraction actions of the actuator to realize the driving control of the end effector. The height of the actuator increases during the inflation period and is shortened during the contraction period. The length and width of the actuator are shortened during the inflation period and elongated during the contraction period. It is assumed that the volume of the actuator remains to be V_1 during the inflation expansion period and the exhaust contraction period, whereas the entire capsule wall thickness is changed uniformly.

3. Output Force Model of CTSPA

In the study, the combination of analytical and experimental methods was used to explore the static characteristic model of the actuator. In the ideal static mathematical model of the soft pneumatic actuator, the structural characteristics are ignored and the law of conservation of energy is used to establish the mathematical relationship between output force, air pressure, and deformations.

The actuator is regarded as an energy conversion unit. When the actuator is inflated, the gas pressure energy applied on the inner surface of the actuator is converted into

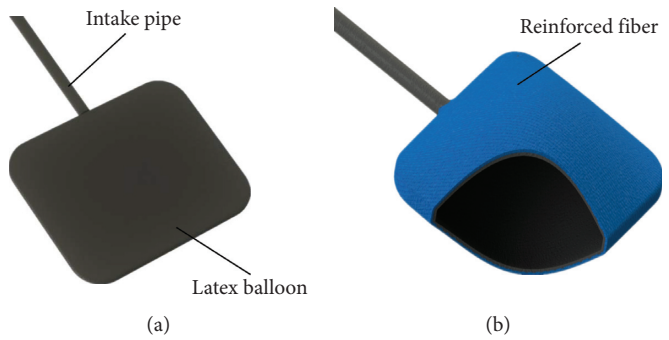

Figure 1: Schematic diagram of the actuator structure.

the mechanical energy, so that the actuator is inflated and rises. According to the principle of virtual work [29], the input work can be expressed as

$$d_{\text{Winput}} = pdV, \tag{1}$$

where p is the absolute pressure inside the CTSPA chamber and dV is the volume change of the CTSPA chamber.

The output work can be expressed as

$$d_{\text{Wout}} = -p_{\text{Ideal}}dh, \tag{2}$$

where F_{Ideal} is the ideal output force of the CTSPA and dh is the height changes of the CTSPA.

According to any small-displacement section of the actuator driving system, if the system loss is zero and there is no energy storage, the input work and output work are the same.

$$d_{\text{Winput}} + d_{\text{Wout}} = 0. \tag{3}$$

After substituting (1) and (2) into (3), the ideal driving force F_{Ideal} of the actuator is obtained as

$$F_{\text{Ideal}} = p\frac{dV}{dh}. \tag{4}$$

In pneumatic drive systems, air pressure and contact area are key factors determining the drive force. Here, the actuator is flexible and the contact area is constantly changed due to the influences of internal air pressure and external load, so the actuator can be regarded as a variable-section cylinder [15].

Therefore, the ideal static mathematical model of the actuator is expressed as

$$F_{\text{Ideal}} = p\overline{A}, \tag{5}$$

where $\overline{A}$ is the equivalent contact area of the CTSPA.

Since the fiber cloth material is strong and sewn with a sewing machine, it can be assumed that the area of fiber cloth is constant during the inflation process of the actuator. In other words, the length and width of the fiber cloth remain unchanged.

The actuator output force model is based on the following assumptions. Firstly, the actuator is uniformly stressed. Secondly, according to the self-made CTSPA structure, the actuator and the connecting plate have a rectangular contact shape during the inflation process and the contact area is related to the inflation pressure and the load. Thirdly, in the expanded state, the wall thickness of the actuator is ignored and the vertical section of the portion, which is not in contact with the connecting plate, is circular, as shown in Figure 2.

As shown in Figure 2, the geometric relationship of the longitudinal section of the actuator under inflation is expressed as

$$D_1 = 2\pi \times \left(\frac{h}{2}\right), \tag{6}$$

$$a_1 = a_3 + 2 \times \left(\frac{D_1}{4}\right), \tag{7}$$

$$a_2 = a_3 + 2 \times \left(\frac{h}{2}\right), \tag{8}$$

where D_1 is the perimeter of the vertical section of the fiber cloth along the longitudinal direction where the cloth is not in contact with the connection plate in the inflated state of the actuator; h_0 is the initial height of the actuator; h is the height of the actuator after inflation; a_2 is the length of the actuator after inflation; a_3 is the contact length of the actuator and the connecting plate in longitudinal direction after inflation.

Similarly, the geometric relationship of the cross section in the width direction of the actuator under inflation is expressed as

$$b_1 = b_3 + 2 \times \left(\frac{D_2}{4}\right), \tag{9}$$

$$b_2 = b_3 + 2 \times \left(\frac{h}{2}\right), \tag{10}$$

where D_2 is the circumferential length of the vertical section in the width direction, and $D_1 = D_2$; b_2 is the width of the actuator after inflation; b_3 is the contact length between the actuator and the connecting plate in the width direction after inflation.; F is the external load.

After substituting (6)~(10) into (5), the output force of the actuator is expressed as

$$F_{\text{Ideal}} = \frac{\pi^2}{4}ph^2 - \frac{\pi(a_1 + b_1)}{2}ph + a_1b_1p, \tag{11}$$

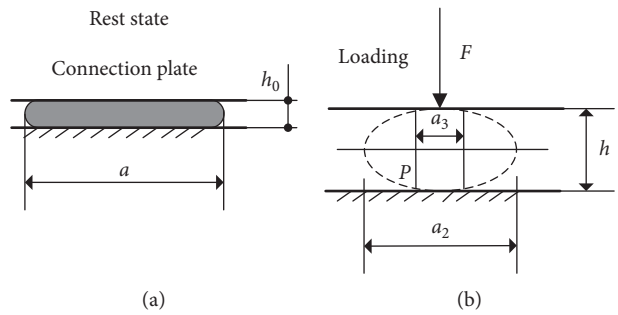

Figure 2: Schematic diagram of the geometry of the longitudinal direction of the actuator.

The actual shape of the fiber cloth, which is not in contact with the connecting plate in the inflated state of the actuator, is related to the load and the pressure in the cavity of the actuator. According to the structural form of the actuator, it is more suitable to be represented by ellipse, but the elliptical circumference has no precise elementary function. Therefore, the expression is approximated as a circle here and corrected with a given coefficient.

Therefore, the output force correction model of the actuator is expressed as

$$F_{\text{Corrected}} = \frac{\gamma\pi^2}{4} ph^2 - \frac{\gamma\pi(a_1 + b_1)}{2} ph + \gamma a_1 b_1 p, \quad (12)$$

where γ is the correction coefficient and can be determined experimentally.

In addition, considering the influences of the colloidal elastic force and the frictional force between the fiber cloth and the surface of the actuator during the actual expansion, the model of the output force of the actuator is further improved as

$$F_{\text{Improved}} = \frac{\gamma\pi^2}{4} p(\zeta h)^2 - \frac{\gamma\pi(a_1 + b_1)}{2} p(\zeta h) + \gamma a_1 b_1 p, \quad (13)$$

where ζ is the correction proportional coefficient of the height of the actuator expansion and can be determined experimentally.

According to (13), the output thrust force of the actuator is related to the air pressure in the chamber, the effective contact area of the actuator, and the load. When the load is constant, the air pressure in the actuator chamber is increased, and the working area is reduced. When the air pressure in the actuator chamber is decreased, the working area is increased. Therefore, the correction coefficient γ and the balloon expansion height proportional coefficient ζ are related to inflation air pressure, load amplitude, and load application position. In addition, the coefficient values of the actuator are also related to its structural parameters. Moreover, the characteristics of the latex balloon material may be changed after a certain period and corresponding parameters are also changed.

4. Simulation and Experimental Study on Static Characteristics of CTSPA

A static mathematical model of the CTSPA is established above and the calculation expression of the output force of the actuator is given. In order to verify the model and explore the relationship between the output force of the actuator, the inflation height, and inflation pressure, with a self-made actuator as the object, the static characteristics were simulated and experimentally investigated.

The static characteristic experiments of the actuator included the static isobaric characteristic experiment, the static isometric characteristic experiment, and the static isotonic characteristic experiment. The static isobaric characteristic experiment explored the relationship between the output thrust of the actuator and the expansion height under a certain inflation pressure. The static isometric characteristic experiment explored relationship between the inflation pressure of the actuator and the output thrust at a certain expansion height. The static isotonic characteristic experiment explored the relationship between the inflation pressure and the expansion height of the actuator under a certain load. The experimental details are given below.

4.1. Static Isobaric Characteristics of CTSPA. The experimental device for static isobaric characteristics of the actuator is shown in Figure 3. It is mainly composed of latex balloon covered with the fiber cloth material, air source, decompression valve (SMC, IR1000-01), force sensor, air pressure sensor, laser displacement sensor, and load cylinder. The air source was an air compressor. A decompression valve was connected between the actuator and the compressor to provide a stable pressure. In order to facilitate the loading process, the load was applied by a cylinder, and a decompression valve was connected between the cylinder and the air source to adjust the load value.

In the experiment, the opening degree of the decompression valve was adjusted and the air pressure was set. After the gas entered the actuator chamber, the actuator was inflated, so that the pressure in the actuator chamber was increased. The actuator inflation height was recorded when the pressure in the actuator chamber was stable. At this point, the actuator inflation expanded and the driving load reached the equilibrium state. Then, the air pressure in the cylinder was continuously adjusted, and the actuator inflation heights under the same inflation pressure were recorded. Through adjusting the opening degree of the decompression valve and changing the inflation air pressure, the above steps were repeated to complete the static isobaric characteristic experiment of the actuator. The coefficient

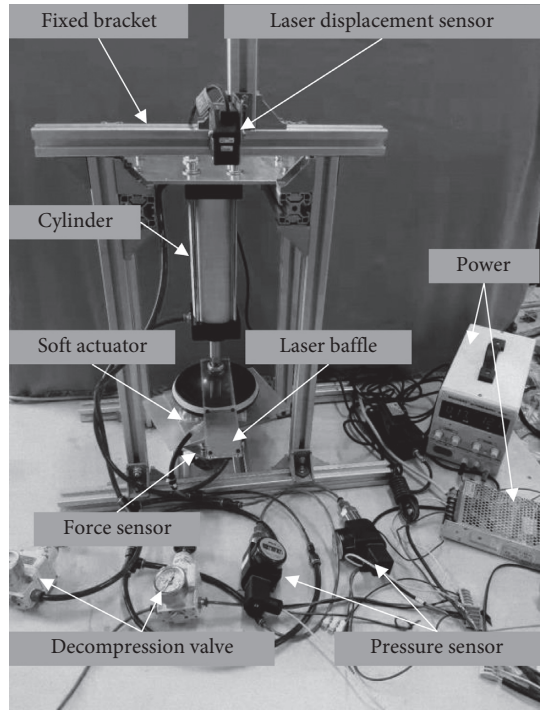

Figure 3: Experimental device for static isobaric characteristics of the actuator.

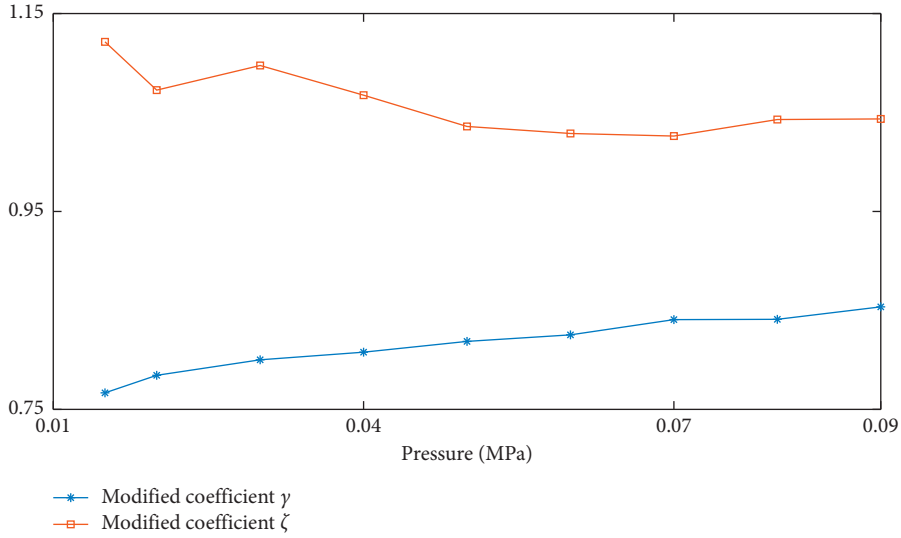

Figure 4: Values of the correction coefficient under different inflation pressures of the actuator.

values of a self-made CTSPA used in this study were solved by the numerical solution based on static isobaric characteristic experiments (Figure 4).

Figure 5 shows the relationship between the actuator inflation height and output force under nine air pressures. The results of the improved output force model of the actuator were closer to the experimental results and the improved model could reflect the static characteristics of the actuator. As the inflation pressure of the actuator increased, the difference between the ideal model and the improved model became smaller, indicating that, under the large inflation pressure, the working area of the actuator in the static isobaric was closer to that in the ideal state. The actuator expansion height decreased with the increase in the load under a certain inflation pressure (Figure 5).

4.2. Static Isometric Characteristics of CTSPA. The experimental device of the static isometric characteristics of the actuator is an improved device, as shown in Figure 3. The air source was connected to the rod cavity of the cylinder. The distance between the end of the cylinder rod and the force

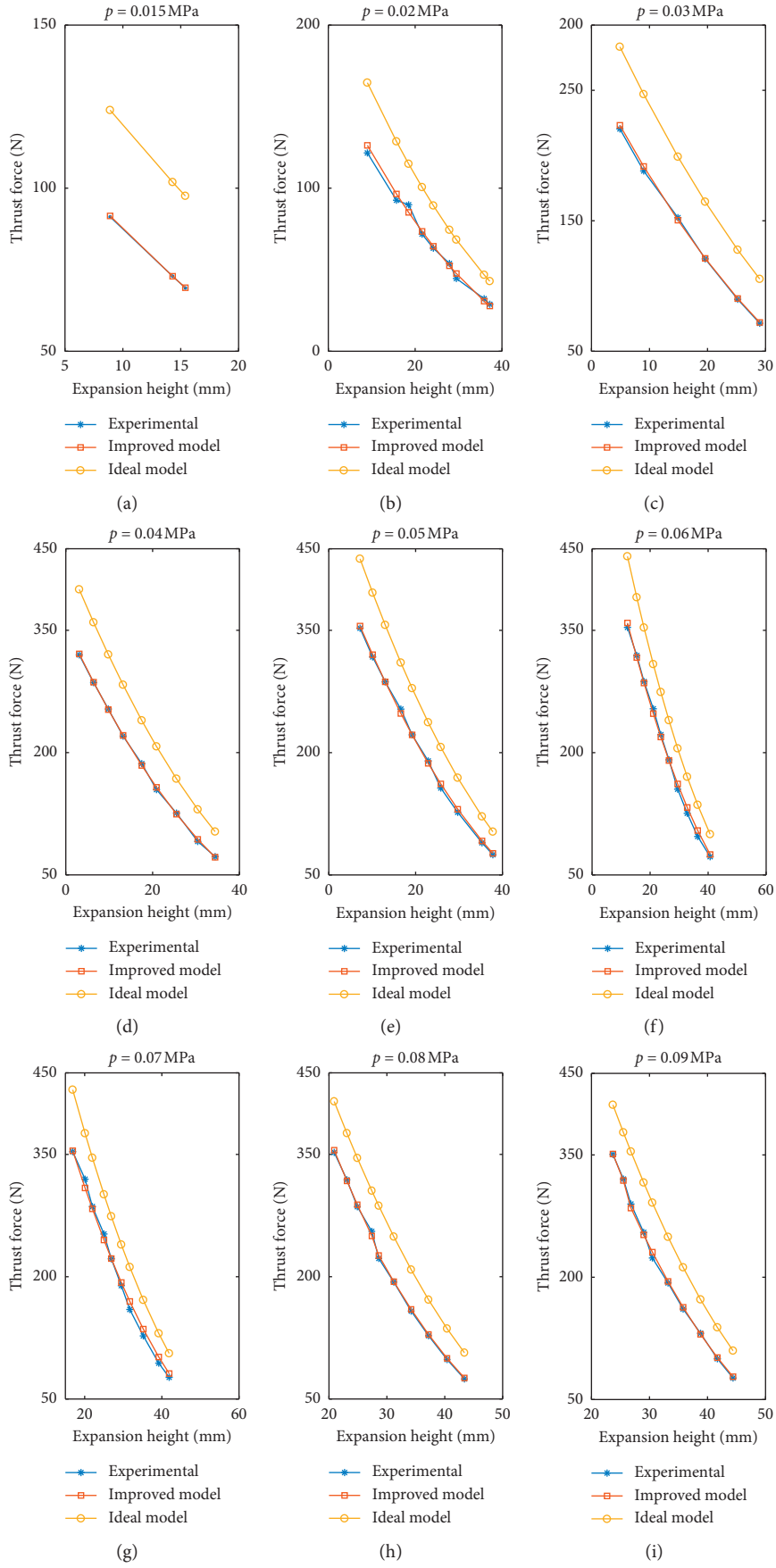

Figure 5: Static isobaric characteristic curve of the actuator.

sensor remained unchanged and the displacement between the actuator and the force sensor was adjusted by applying blocks, thereby changing the inflation level of the actuator. In the experiment, after the adjustment block was placed, the actuator chamber was continuously filled with gas and the actuator output thrust was recorded. Figure 6 shows the relationship between the actuator inflation pressure and output force under six inflation heights of the actuator based on the ideal output force calculation model, the improved output force calculation model, and the experimental measured values. When the inflation expansion height of the actuator was constant, the actuator output force was proportional to the inflation air pressure. However, under the large inflation pressure, the difference between the experimental value and the simulated calculation value increased. The difference might be interpreted as follows. The correction coefficients were measured under specific pressure state and certain loads in the laboratory, thus resulting in large calculation errors. However, the improved output force model could still better reflect the static characteristics of the actuator. The correction coefficients will be further serialized in the future.

4.3. Static Isotonic Characteristics of CTSPA. The experimental device of the static isotonic characteristics of the actuator was the same as the device of the static isobaric characteristics experiments. Firstly, the decompression valve threshold between the air source and the cylinder was set. The cylinder provided a certain load and the actuator chamber was continuously filled with gas. The expansion height of the actuator was recorded. Subsequently, the threshold value of the decompression valve was adjusted and the experimental process was repeated. Figure 7 shows the relationship between the actuator inflation air pressure and the actuator inflation height under six external loads based on the ideal output force calculation model, the improved output force calculation model, and the experimental measured values. When the actuator output thrust was less than external load, the inflation height of the actuator was zero. Then the actuator firstly expanded rapidly and subsequently expanded smoothly. The results of the improved output force model of the actuator were closer to the experimental results.

5. Experimental Study on Dynamic Characteristics of CTSPA

5.1. Response Characteristics of CTSPA. Many factors affect the performance of the pneumatic control system, such as air source pressure, gas flow, and working load. These factors have a complicated impact on the system performance. Therefore, it is necessary to further study the dynamic response characteristics of the CTSPA for the controller design of pneumatic drive system.

In general, one-step signals contain break points, which are the severe operating condition of the control system. The zero-state response generated by the system under the action of the step signal can largely reflect the dynamic characteristics of the system. Therefore, the step response method was used to analyze the dynamic characteristics of the open-loop control system of the CTSPA. Under a constant load, after the supply pressure was stabilized, a one-step signal was given to the proportional valve to explore the inflating and exhausting characteristics of the actuator. The experimental device of the dynamic characteristics of the soft pneumatic actuator control system was similar with the device shown in Figure 3. As shown in Figure 8, it is mainly composed of controller, signal processing module, decompression valve, proportional valve, laser displacement sensor, CTSPA, and load.

Under the same loading state (70 N) and six air pressures (15, 25, 40, 70, 90, and 100 kpa), the experiments were performed to analyze the dynamic characteristics of the open-loop control system of the CTSPA. After the load was applied and the supply pressure was stabilized, a command signal was input into the controller and a step signal was instantaneously given to the No. 1 proportional valve, so that the inflation valve spool was opened. Then the compressed gas entered the actuator chamber, and the actuator expanded to a stable position. Then, another command signal was input into the controller, so that the valve core of the No. 1 inflation proportional valve was closed. A step signal was given to the No. 2 proportional valve instantaneously, so that the valve core of the exhaust valve was opened. After the gas in the actuator chamber was exhausted, the air pressure was reduced to zero (the gauge pressure). Then the actuator shrunk to its initial position, thus completing a working cycle of the CTSPA. In a whole cycle, the changes of air pressure in the actuator chamber and the actuator displacement were detected by air pressure sensor and laser displacement sensor in real time. Through changing the operating conditions of the control system of the CTSPA and repeating the experimental working cycle, the dynamic characteristic experiments of the actuator were performed.

Figure 9 shows the pressures in CTPSA and expansion heights under six inflation pressures. After the core of the inflation valve was opened, compressed air entered the actuator. The air pressure in the chamber increased rapidly, whereafter the intake air speed became slow. The change might be interpreted as follows. After the inflation valve was opened, the upstream air of the No. 1 proportional valve was instantaneously released and the inflation pressure was instantaneously decreased. Then the air source supplemented the air pressure to the set value. In the process of inflation and expansion, a part of the gas energy was converted into elastic energy. The obvious hysteresis phenomenon was observed in the experimental curves. With the increase in the pressure in the actuator chamber, it was difficult to fill gas into the chamber, thus leading to the slower increase rate of the pressure in the later stage. Under the same load, the inflation pressure was larger and equilibrium time was shorter. When exhaust gas was contracted, the air pressure in the actuator chamber dropped slowly to zero in the later stage. The output displacement was the

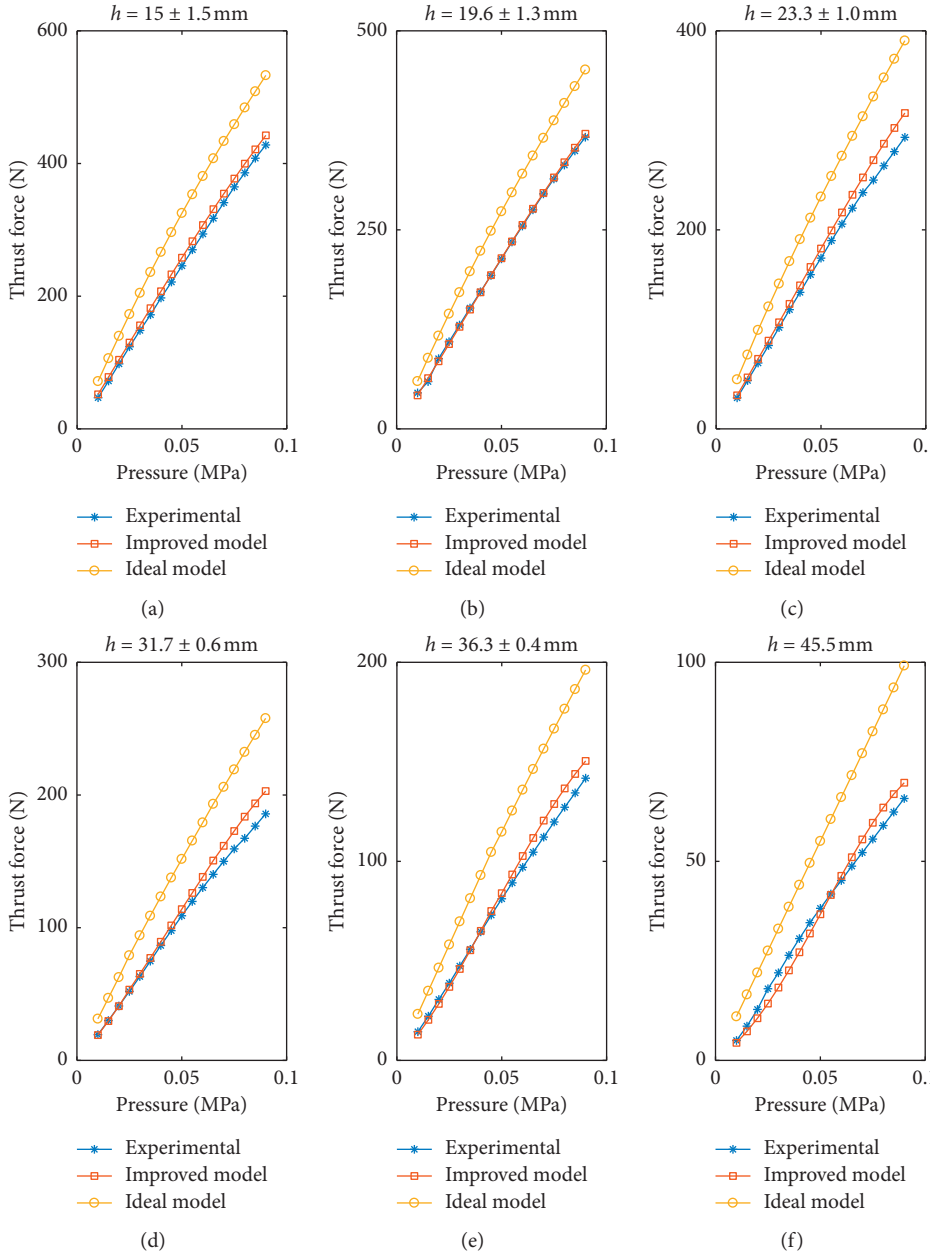

Figure 6: Static isometric characteristics curve of the actuator.

combined consequence of load, effective contact area, and pressure in the chamber.

Figure 10 shows the hysteresis results of the CTSPA. The relative relationship between the parameters was more complicated. When the actual control system was used, the intermediate inflation stage of the actuator could be fully utilized. Several actuators could be stacked in series to meet the requirements.

It can be seen from the above analysis that the dynamic characteristics of the CTSPA are strongly influenced by the factors of the control system, such as air supply, inflation pressure, material characteristics and structural parameters of the actuator, and load. Thus, the CTSPA control system was relatively complicated.

5.2. Position Tracking of CTSPA. In our previous study, the CTSPA has been used to develop a robot-assisted system to achieve and maintain anatomic or functional reduction of femoral shaft fractures [30]. Here, the position control of CTSPA was carried out by fuzzy proportional-derivative closed-loop control in the testbed shown in Figure 11. The testbed for the position control has a single joint, which rotates from 0 to 10°. The rubber strips provide the resistance

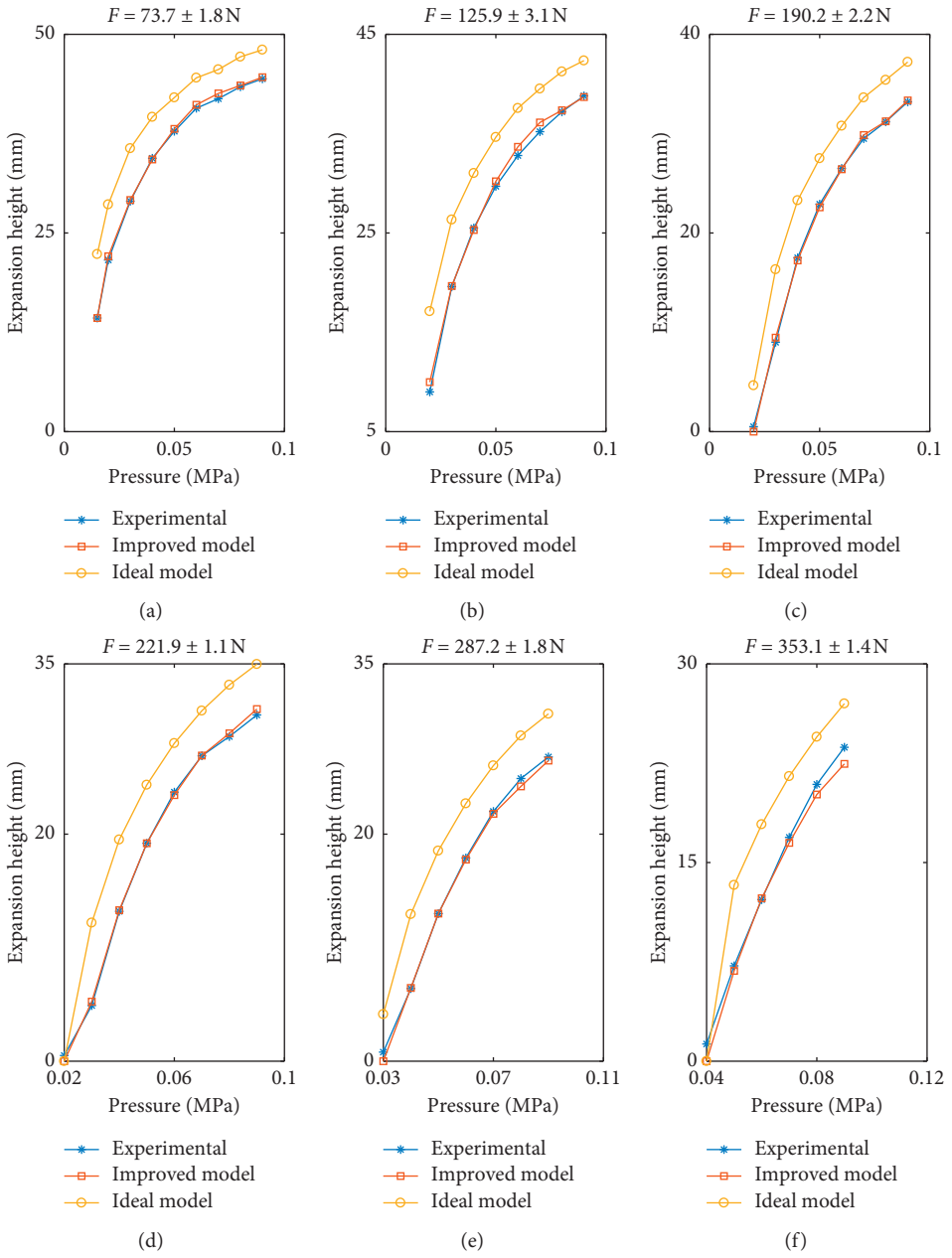

Figure 7: Static isotonic characteristic curve of the actuator.

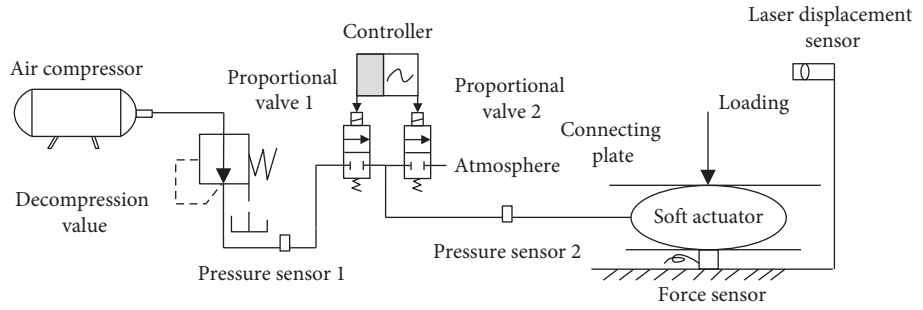

Figure 8: Schematic diagram of the experiment device of the dynamic characteristics of the actuator.

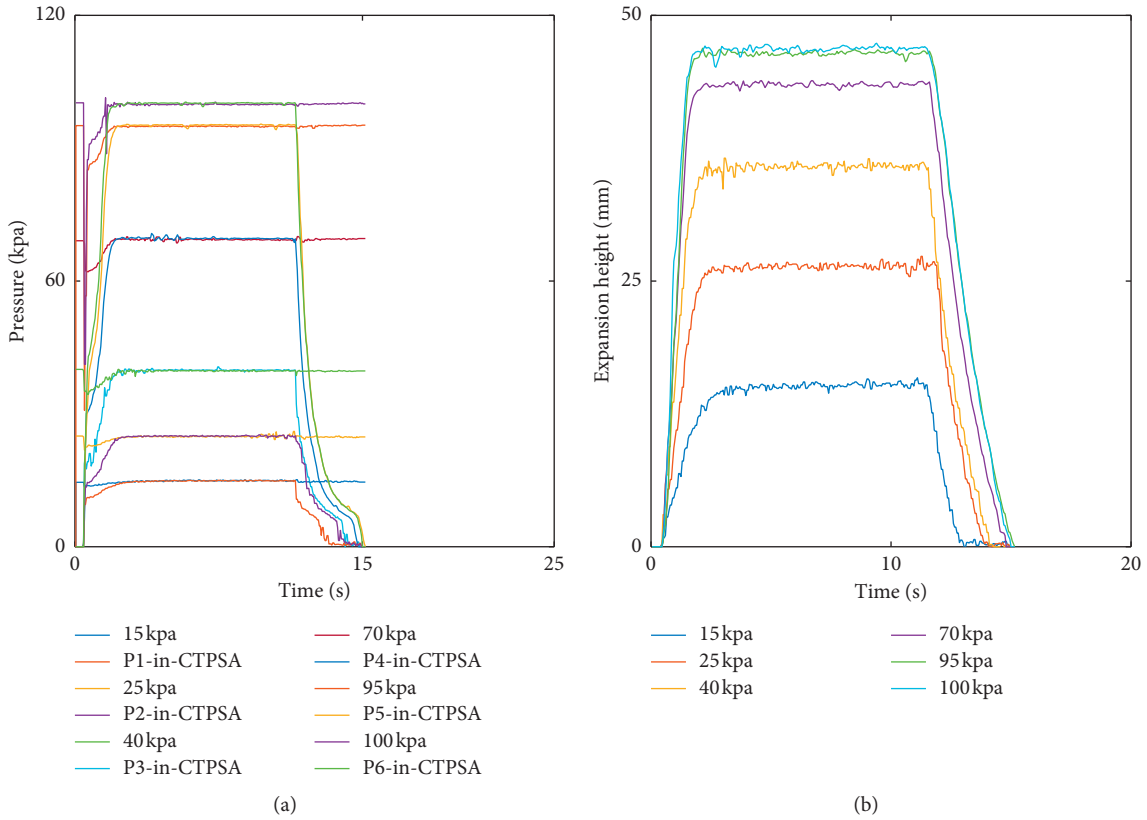

Figure 9: Pressures in CTPSA and expansion heights under six inflation pressures.

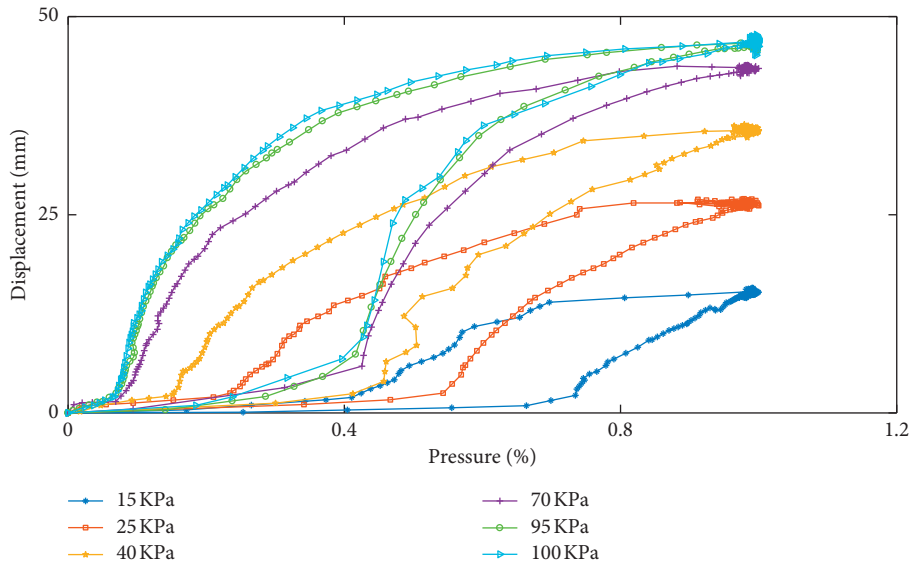

Figure 10: Hysteresis test results.

against the joint rotation. The angle sensor records angle changes in real time.

Given the equation for joint angle,

$$\begin{cases} \theta(t) = 195.3t^3 - 366.2t^4 + 183.1t^5, & t \in [0, 0.8\,\text{s}], \\ \theta(t) = 100t^3 - 150t^4 + 60t^5, & t \in [0, 1\,\text{s}]. \end{cases} \tag{14}$$

Figure 12 shows the position tracking performance of CTSPA at 1 Hz and 1.25 Hz. The average errors were, respectively, 0.3° and 0.67° and the maximum errors were, respectively, 0.75° and 1.6°. With the increase in the frequency of the input signal, the influence of the hysteresis on tracking the target curve increased, thus decreasing the tracking performance of CTSPA.

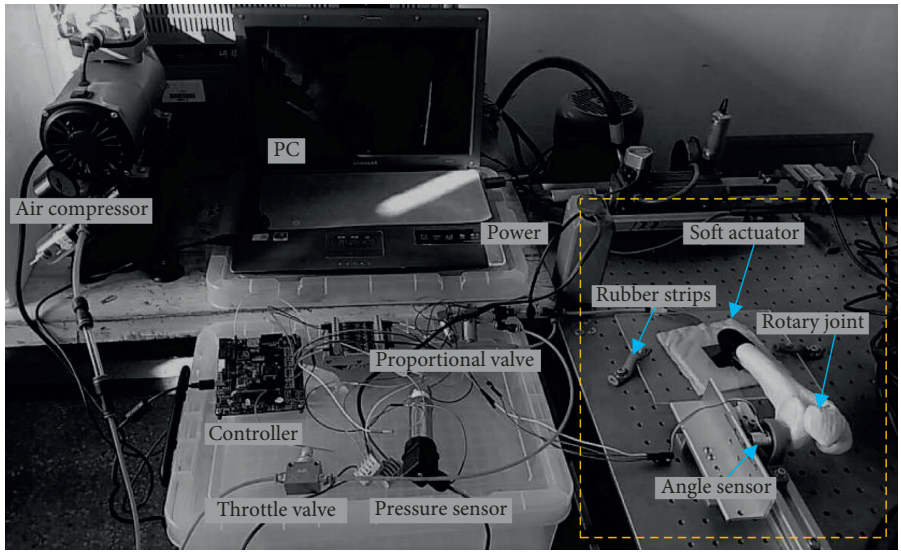

Figure 11: Experimental device for position tracking performance.

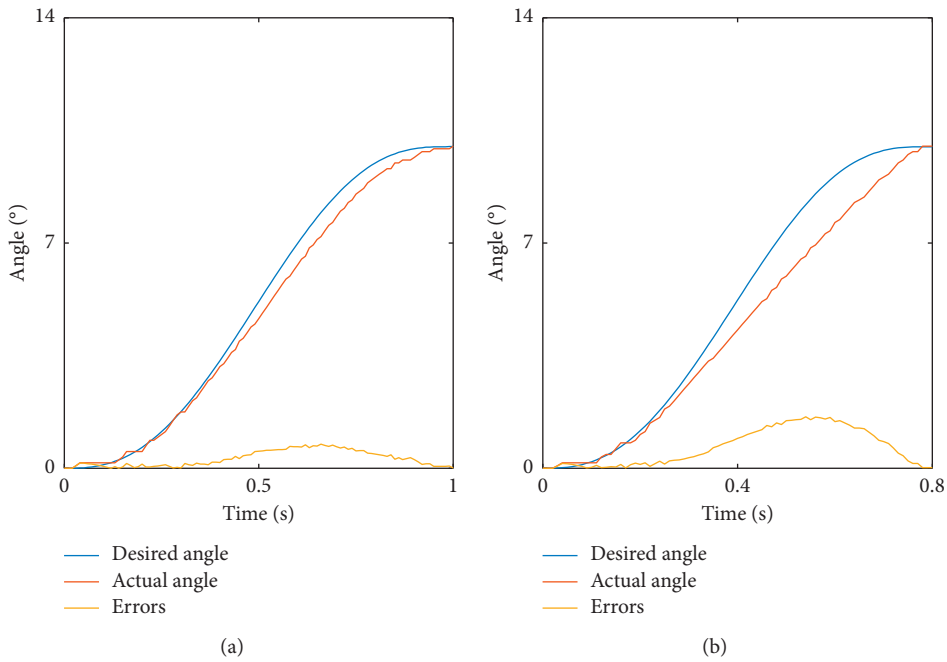

Figure 12: Position tracking with fuzzy PID algorithm. (a) 1 Hz and (b) 1.25 Hz.

6. Conclusions

The soft contact characteristics and continuous deformation capability of soft robots are significant for the application of nonlinear soft materials. The high deformation capacity, large displacement, and large thrust characteristics of soft robots can be extended to more application fields, such as rehabilitation/assisted medical, radiation operations, and compression hemostasis in military areas. Based on the ultra-high elastic deformation ability of latex materials, combined with high-strength and high-modulus fiber materials, the high-elasticity soft pneumatic actuator was prepared to meet the strict demands of working space and provide large stroke and large thrust. In this study, the static characteristics of the high-elasticity soft pneumatic actuator were explored by analytical and experimental methods. The static characteristic mathematical model was established and experimentally verified. Subsequently, the dynamic response characteristics of the CTSPA were explored by means of experimental analysis. It is well known that the nonlinear problem of the soft actuator covering fiber fabric was quite prominent. Finally, the effect of CTSPA on the input signal was studied with the Fuzzy-PD control algorithm. With the increase in the frequency of the input signal, the tracking performance of CTSPA deteriorated due to the impact of hysteresis. The results provided

the theoretical basis for the future design of flexible drive systems.

However, the latex material has the phenomenon of aging, indicating that the latex product is affected by various conditions of natural and artificial environments during storage and use. The performance and appearance deteriorate with time, and corresponding parameters also change. In order to prevent or delay the aging tendency, it is necessary to reduce the influences of sunlight, wind, rain, and other factors and add antiaging agents when formulating the rubber compound.

Furthermore, the correction coefficient γ and the balloon expansion height proportional coefficient ζ are the key parameters to be determined in pneumatic drive systems. The actuators with different structural parameters have different coefficient values and the quantity of samples affects the determined values of the two coefficients. In the future, the performance of several actuators superimposed together will be explored and a reasonable method will be developed to solve the parameters.

Data Availability

The data used to support the findings of this study are included within the article.

Conflicts of Interest

The authors declare that there are no conflicts of interest regarding the publication of this paper.

Acknowledgments

The authors are grateful to the anonymous reviewers and the editor for their constructive comments. This work was supported by Anhui Science and Technology Major Project (201903a05020029), the University Synergy Innovation Program of Anhui Province (GXXT-2019-048), the Fundamental Research Funds for Young Teachers of Anhui University of Technology (QZ201809), and the Fundamental Research Funds for the Central Universities, the Graduate Student Scientific Research Innovation projects of General University of Jiangsu Province (KYLX_0101).

References

[1] Z. Q. Zhang, J. Zou, J. N. Ding et al., "Research status of the soft robot driving," *Robot*, vol. 40, no. 5, pp. 648–659, 2018.

[2] C. Zhang, "Simulation analysis of bionic robot fish based on MFC materials," *Mathematical Problems in Engineering*, vol. 2019, Article ID 2720873, 9 pages, 2019.

[3] F. Daerden and D. Lefeber, "Pneumatic artificial muscles: actuators for robotics and automation," *European Journal of Mechanical and Environmental Engineering*, vol. 47, no. 1, pp. 11–21, 2002.

[4] M. T. Tolley, R. F. Shepherd, B. Mosadegh et al., "A resilient, untethered soft robot," *Soft Robotics*, vol. 1, no. 3, pp. 213–223, 2014.

[5] K. C. Galloway, K. P. Becker, B. Phillips et al., "Soft robotic grippers for biological sampling on deep reefs," *Soft Robotics*, vol. 3, no. 1, pp. 23–33, 2016.

[6] N. Y. Wang, H. Sun, H. Jiang et al., "On grasp strategy of honeycomb pneunets soft gripper," *Robot*, vol. 38, no. 3, pp. 371–377, 2016.

[7] N. W. Bartlett, M. T. Tolley, J. T. B. Overvelde et al., "A 3D-printed, functionally graded soft robot powered by combustion," *Science*, vol. 349, no. 6244, pp. 161–165, 2015.

[8] M. Wehner, R. L. Truby, D. J. Fitzgerald et al., "An integrated design and fabrication strategy for entirely soft, autonomous robots," *Nature*, vol. 536, no. 7617, pp. 451–455, 2016.

[9] C. P. Chou and B. Hannaford, "Measurement and modeling of McKibben pneumatic artificial muscle," *IEEE Transactions on Robotics and Automation*, vol. 12, no. 1, pp. 90–102, 1996.

[10] K. Liu, T. Ma, B. Gu, Y. Wang, D. Zhao, and Y. Lu, "A new method to predict contractile force for pneumatic muscle actuators," *Advanced Robotics*, vol. 29, no. 17, pp. 1127–1136, 2015.

[11] G. Andrikopoulos, G. Nikolakopoulos, and S. Manesis, "Novel considerations on static force modeling of pneumatic muscle actuators," *IEEE/ASME Transactions on Mechatronics*, vol. 21, no. 6, pp. 2647–2659, 2016.

[12] H. Al-Fahaam, S. Nefti-Meziani, T. Theodoridis, and S. Davis, "The design and mathematical model of a novel variable stiffness extensor-contractor pneumatic artificial muscle," *Soft Robotics*, vol. 5, no. 5, pp. 576–591, 2018.

[13] J. Zhao, J. Zhong, and J. Fan, "Position control of a pneumatic muscle actuator using RBF neural network tuned PID controller," *Mathematical Problems in Engineering*, vol. 2015, Article ID 810231, 16 pages, 2015.

[14] J. E. Takosoglu, P. A. Laski, S. Blasiak, G. Bracha, and D. Pietrala, "Determining the static characteristics of pneumatic muscles," *Measurement and Control*, vol. 49, no. 2, pp. 62–71, 2016.

[15] G. Yang, B. R. Li, and X. Y. Fu, "Research on dynamic characteristics of a pneumatic muscle actuator," *China Mechanical Engineering*, vol. 17, no. 12, pp. 1294–1298, 2006.

[16] J. M. Du, D. Y. Zhu, G. Yang et al., "Experimental research on the static characteristic of pneumatic muscle actuator," *Machine Tool & Hydraulics*, vol. 5, pp. 21–23, 2005.

[17] Y. Teng, G. Yang, X. N. Li et al., "Development and characteristics of pneumatic compliant actuator with thrust force and large stroke output," *Journal of Nanjing University of Science and Technology*, vol. 35, no. 4, pp. 502–506, 2011.

[18] G. Belforte, G. Eula, A. Ivanov, and A. L. Visan, "Bellows textile muscle," *The Journal of The Textile Institute*, vol. 105, no. 3, pp. 356–364, 2014.

[19] J. G. Lee and H. Rodrigue, "Origami-based vacuum pneumatic artificial muscles with large contraction ratios," *Soft Robotics*, vol. 6, no. 1, pp. 109–117, 2019.

[20] H. D. Yang, B. T. Greczek, and T. A. Asbeck, "Modeling and analysis of a high-displacement pneumatic artificial muscle with integrated sensing," *Frontiers in Robotics and AI*, vol. 5, p. 136, 2019.

[21] Y. Du, B. Liu, M. Xu, E. Dong, S. Zhang, and J. Yang, "Dynamic characteristics of planar bending actuator embedded with shape memory alloy," *Mechatronics*, vol. 25, pp. 18–26, 2015.

[22] C. A. Vivas-Lopez, J. C. Tudon-Martinez, D. Hernandez-Alcantara, and R. Morales-Menendez, "Global chassis control system using suspension, steering, and braking subsystems," *Mathematical Problems in Engineering*, vol. 2015, Article ID 905731, 18 pages, 2015.

[23] A. Oonishi, K. Hirata, B. Yoo et al., "Frequency response characteristics for linear actuator made by NiMnGa shape memory alloy," *International Journal of Applied Electromagnetics and Mechanics*, vol. 39, no. 1–4, pp. 913–918, 2012.

[24] G. Zhao, J. J. Yang, Y. J. Wang et al., "Investigation into response characteristics of the chitosan gel artificial muscle," *Smart Materials and Structures*, vol. 27, no. 1, Article ID 015001, 2018.

[25] H. J. Kim, W. S. Yang, and K. No, "Effects of an elastic mass on frequency response characteristics of an ultra-thin piezoelectric micro-acoustic actuator," *IEEE Transactions on Ultrasonics, Ferroelectrics and Frequency Control*, vol. 60, no. 8, pp. 1587–1594, 2013.

[26] U. Gupta, Y. Wang, H. Ren, and J. Zhu, "Dynamic modeling and feedforward control of jaw movements driven by viscoelastic artificial muscles," *IEEE/ASME Transactions on Mechatronics*, vol. 24, no. 1, pp. 25–35, 2019.

[27] J. Sarosi, I. Biro, J. Nemeth, and L. Cveticanin, "Dynamic modeling of a pneumatic muscle actuator with two-direction motion," *Mechanism and Machine Theory*, vol. 85, pp. 25–34, 2015.

[28] A. J. Veale, S. Q. Xie, and I. A. Anderson, "Modeling the Peano fluidic muscle and the effects of its material properties on its static and dynamic behaviour," *Smart Materials and Structures*, vol. 25, no. 6, Article ID 065014, 2016.

[29] K. Han, N.-H. Kim, and D. Shin, "A novel soft pneumatic artificial muscle with high-contraction ratio," *Soft Robotics*, vol. 5, no. 5, pp. 554–566, 2018.

[30] Q. Zhu, B. Liang, X. Wang, X. Sun, and L. Wang, "Minimally invasive treatment of displaced femoral shaft fractures with a teleoperated robot-assisted surgical system," *Injury*, vol. 48, no. 10, pp. 2253–2259, 2017.